scientific reports

Check for updates

OPEN

Leucettamine B and nacryline derivative promote the first steps of endochondral ossification in vitro

Capucine Jourdain de Muizon[1,5], Sarah Nahle[2,5], Céline Moriou[1], Sylvain Petek[3], Chaïma El Ouazzani[2], Ali Al Mourabit[1,6] & Marthe Rousseau[2,4,6]✉

Nowadays, there is a lack of pharmacological interventions designed to stimulate endochondral ossification (EO) in long bone fracture healing. In the search for new active compounds, marine organisms, particularly calcarea sponges and pearl oysters were studied. Two natural compounds, leucettamine B and nacryline, were isolated from the sponge *Pericharax orientalis* and the nacre of the pearl oyster *Pinctada margaritifera*, respectively. Interestingly, leucettamine B and nacryline exhibit significant structural similarities. A library of derivatives of both molecules was synthesized. A new synthetic pathway was developed to access leucettamine B and its derivatives via late-functionalization. Four compounds demonstrated activity on the ColX-MetLuc-ATCD5 test at 0.2 mM. Among them, pinctazole, a synthetic analog of nacryline, significantly stimulated matrix mineralization in ATDC5 cells. In silico analysis revealed that this compound may exert multitarget and multipathway regulatory effects on EO. Molecular docking studies showed that pinctazole had the highest binding affinity to Src. Additionally, in silico pharmacokinetic evaluation indicated that this compound might be well absorbed. Overall, our results suggest that pinctazole may play a role in early events associated with EO, an essential process for bone repair.

Keywords Leucetammine B, Sponges, Nacre, Endochondral ossification

Bone fractures are a global health concern, often leading to disability, prolonged recovery, and a significant financial burden on affected individuals. Although bone has the capacity for full regeneration, complications such as delayed healing or nonunion occur in approximately 5–10% of cases[1]. Long bone fractures typically heal through endochondral ossification (EO), a fundamental process in skeletal development, in which cartilage is gradually degraded and replaced by bone. Despite the crucial role of EO in the successful fracture repair, therapeutic approaches have traditionally focused on stimulating intramembranous ossification using the bone morphogenetic proteins and stabilizing the fracture site[2]. The search for new active molecules targeting EO has led to the discovery of several marine metabolites showing promising in vivo and in vitro activities[3].

Nacre, also known as mother-of-pearl, is produced by some mollusk and is considered a biocompatible material studied for its potential as a bone substitute. In addition to its structural properties, nacre has been shown to exhibit osteoinductive effect[4]. The impact of nacre powder on bone was shown to be a safe biomaterial for bone regeneration in a sheep model[5]. To date, only a few small compounds were identified in the organic matrix of nacre[6]. Uncovering the active metabolites present in this marine biomaterial could lead to the discovery of new organic compounds to treat bone nonunion.

Beyond mollusks, other marine organisms also hold osteogenic properties. Among 47 sponges from Wallis Island screened for their bone-related activity, two calcareous sponges exhibited the highest effect. Calcareous sponges are one of the four classes within the Porifera phylum. They produce a mineralized skeleton mainly composed of calcium carbonate. These two sponges, belonging to the *Pericharax* and *Leucetta* genus have

[1]CNRS, Institut de Chimie des Substances Naturelles, Université Paris-Saclay, Gif-sur-Yvette F-91190, France. [2]INSERM, Mines Saint Etienne, SAINBIOSE U1059, Université Jean Monnet Saint-Étienne, Saint-Étienne F-42023, France. [3]IRD, CNRS, Ifremer, Univ Brest, LEMAR, IUEM, Plouzane F-29280, France. [4]UMR5510 MATEIS, CNRS/Lyon University/INSA-Lyon, Lyon, France. [5]Capucine Jourdain de Muizon and Sarah Nahle contributed equally to this work. [6]Ali Al Mourabit and Marthe Rousseau: These authors jointly supervised this work. ✉email: marthe.rousseau@univ-st-etienne.fr

previously been studied by our group for the identification of bioactive metabolites with potential effects on bone[7].

Leucettamine B (**1**) was first isolated from the sponge *Leucetta microraphis* in 1993[8]. Several total syntheses have been documented in the litterature[9–11]. Leucettamine B (**1**) and its analogs have been evaluated for their DYRKs /CLKs kinases inhibition[12] and cytotoxicity on MDA-MB-468 cancer cell lines[13], with most compounds showing micromolar and submicromolar IC_{50} values. More recently, leucettamine B (**1**) was screened for its potential involvement in chondrocyte hypertrophic differentiation[7]. However, in that study, the compound was only evaluated in a screening context, and its mechanism of action was not investigated and its analogues were not assessed in this biological context. The investigation of the sponge *Pericharax orientalis* and nacre powder from *Pinctada margaritifera* led to the identification of two compounds showing interesting activity on the first steps of endochondral ossification: leucettamine B (**1**) from the sponge *Pericharax orientalis* and nacryline (**2**) from the nacre of *Pinctada margaritifera*. While leucettamine B (**1**) is a known natural compound, nacryline (**2**), though previously synthesized, had never been identified as a naturally occurring isolated product.

The aim of this study was to identify the most potent analog capable of promoting endochondral ossification.

Results and discussion

Chemical synthesis

Active compounds isolation

The sponge *Pericharax orientalis* was collected from the Wallis Island lagoon during the WALLIS 2018 expedition[14]. Leucettamine B (**1**) was isolated following extraction of the freeze-dried sponge using a CH_2Cl_2/MeOH: 1/1 mixture, followed by *n*-BuOH/H_2O partitioning. To focus on active compounds, the butanolic extract was fractionated using reversed-phase C_{18} flash chromatography and further purified by repetitive preparative C_{18}-HPLC.

Nacre powder was obtained from the shell of *Pinctada margaritifera* oysters, a by-product of the pearl farming industry in the French Polynesia. Organic metabolites of nacre were extracted by pure dichloromethane, and the obtained crude extract was then portioned on silica gel before further purification by repetitive preparative C_{18}-HPLC to isolate nacryline (**2**).

All the pure compounds extracted from the sponge *Pericharax orientalis* and from nacre were evaluated for their activity on endochondral ossification. Notably, leucettamine B (**1**) and nacryline (**2**) share significant structural similarities (Fig. 1).

Since leucettamine B (**1**) and nacryline (**2**) were isolated in limited quantities, their synthesis was necessary for further biological studies. A new total synthesis was developed to access leucettamine B (**1**) and other 6 derivatives. Additionally, the straightforward synthesis of nacryline (**2**) via Knoevenagel condensation was achieved, leading to a library of 17 analogs.

New total synthesis of leucettamine B (1) and its analogues

A previous study has achieved the synthesis of leucettamine B (**1**) through the addition of a substituted guanidine on the oxidated pseudo-diketopiperazine[7,15]. Building on this approach, the 2-aminoimidazolone core can be selectively functionalized with variously substituted guanidines at a late stage. Following this strategy, leucettamine B (**1**) and its derivatives were synthetized.

To obtain the derivatives, the synthetic pathway was applied using MOM-protected tyrosine methyl ester and O-methyltyrosine methyl ester[16]. During the pseudo-peptide cyclization step, partial spontaneous oxidation by air oxygen led to the formation of a rearrangement product **D2** (Fig S1). The structure of this rearranged product was confirmed by X-ray diffraction analysis on the O-Me derivative. Complete oxidation of the corresponding diketopiperazine yielded compound **D1**, which had been previously described[15](Fig S1).

Further experimentation showed that any substituted guanidine reacts with both the oxidated diketopiperazines and their rearrangement compounds, leading to the same final desired 2-aminoimidazolones. Several substituted guanidines were added on both O-Me and O-MOM rearrangement products (compounds **D2** and **D4**), yielding compounds **3** to **8.** When necessary, MOM deprotection was performed quantitatively. Regioisomers **5** and **6** were discriminated using X-ray diffraction analysis of the MOM-protected corresponding compounds (Fig. 2**).**

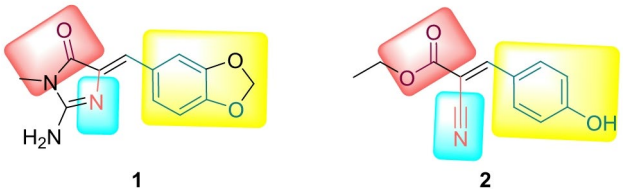

Fig. 1. Structural similarities between leucettamine B (1) and nacryline (2) highlighted by colours. The red region indicates the common carbonyl function, the blue region highlights the nitrogen-containing insaturated bond, and the yellow region corresponds to the aromatic ring system occupying a similar position in both molecules.

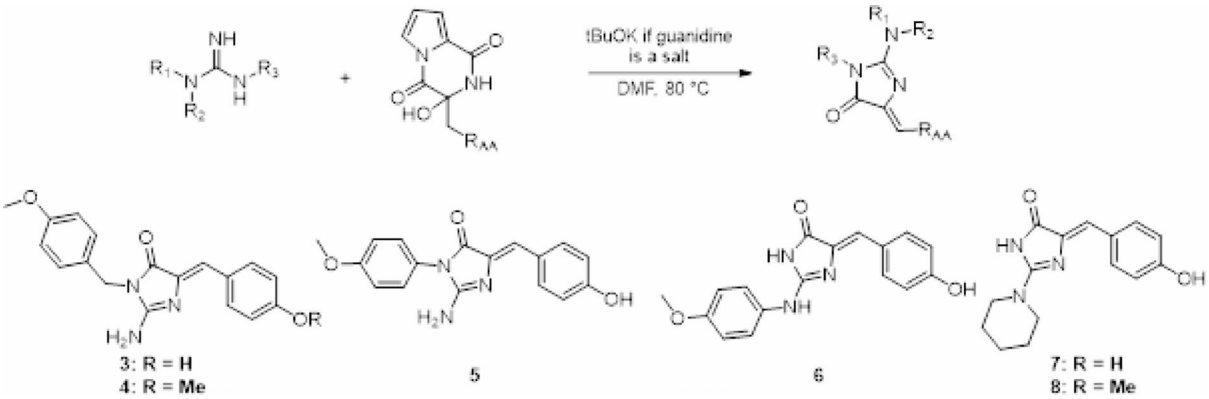

Fig. 2. General synthetic pathway of leucettamine B's analogs and structure of the synthetized analogs. Additional information on analogs is available in the main text.

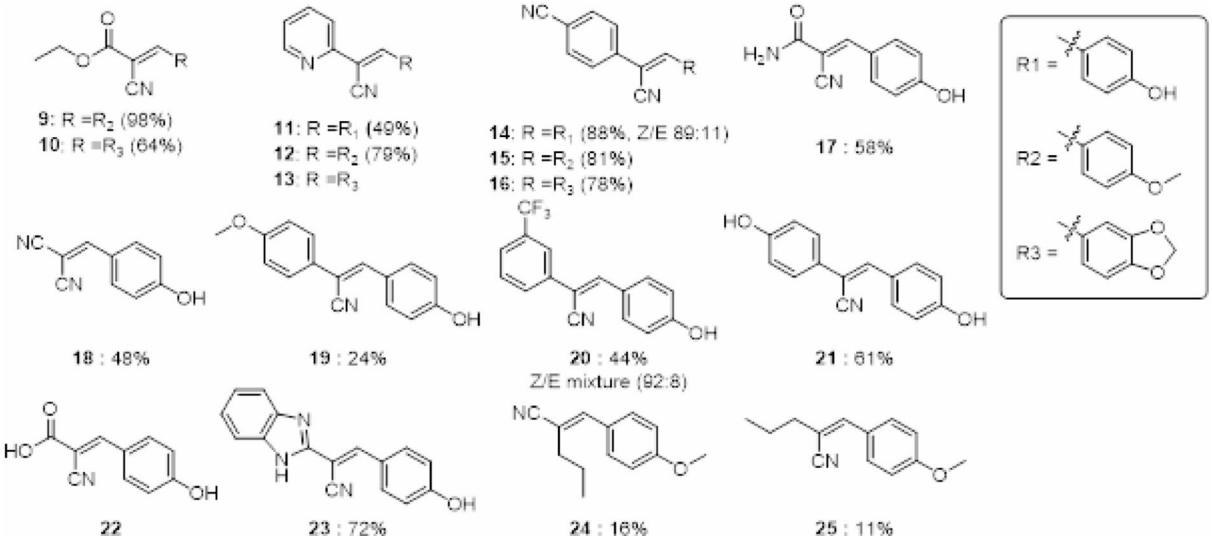

Fig. 3. Structures of the synthetized analogs of nacryline (2). Additional information on analogs is available in the main text.

Synthesis of nacryline (2) and analogues

Nacryline (**2**) and 16 analogues were then synthetized via the simple Knoevenagel condensation, as described by Stevens et al.[16] using hydroxybenzaldehyde, 4-methoxybenzaldehyde and piperonal as starting materials. The structures of the 16 synthetized analogues are shown on Fig. 3. In most cases, only one regioisomer of the alkene was obtained. When a mixture was observed, the (*Z*) and (*E*) regioisomers were not separated and were tested together. When the double bond is substituted by two aromatic rings and a nitrile, the (Z) configuration is preferentially formed. The (*E*) configuration of compounds **2**, **9** and **10** was determined by NOESY NMR experiments (see supplementary data). The *Z* and *E* isomers are clearly distinguishable, as the alkene proton shifts from 7.0 to 7.5 ppm when the cyano is adjacent and from 7.5 to 8.5 ppm when cyano group is positioned next to the aromatic group. Stereochemistry was confirmed by the comparison of our data with the literature values for the known compounds (**9**, **10**, **12**, **15**, **17**, **18** and **21**). Derivatives **24** and **25** were obtained by exposing 4-methoxybenzaldehyde dissolved in pentanenitrile to KOH and were separated by flash chromatography. Compound **22** is commercially available.

Biological activity

Identification of compounds promoting chondrocyte hypertrophic differentiation in vitro

In order to identify compounds able to stimulate hypertrophic differentiation of chondrocytes, we developed a reporter system to measure the transcriptional activity of collagen X, a key marker of hypertrophy. We generated a mouse prechondrogenic ATDC5 cell line, stably expressing ColX-pMetLuc-ATDC5 as described in the Materials and Methods section. The workflow of the biological activity study is illustrated in Fig. 4A.

Using the cell-based screening assay, 4 out of 25 compounds were identified as markedly upregulating Collagen X transcriptional activity (Fig. 4B). Consequently, these compounds were selected for further evaluation

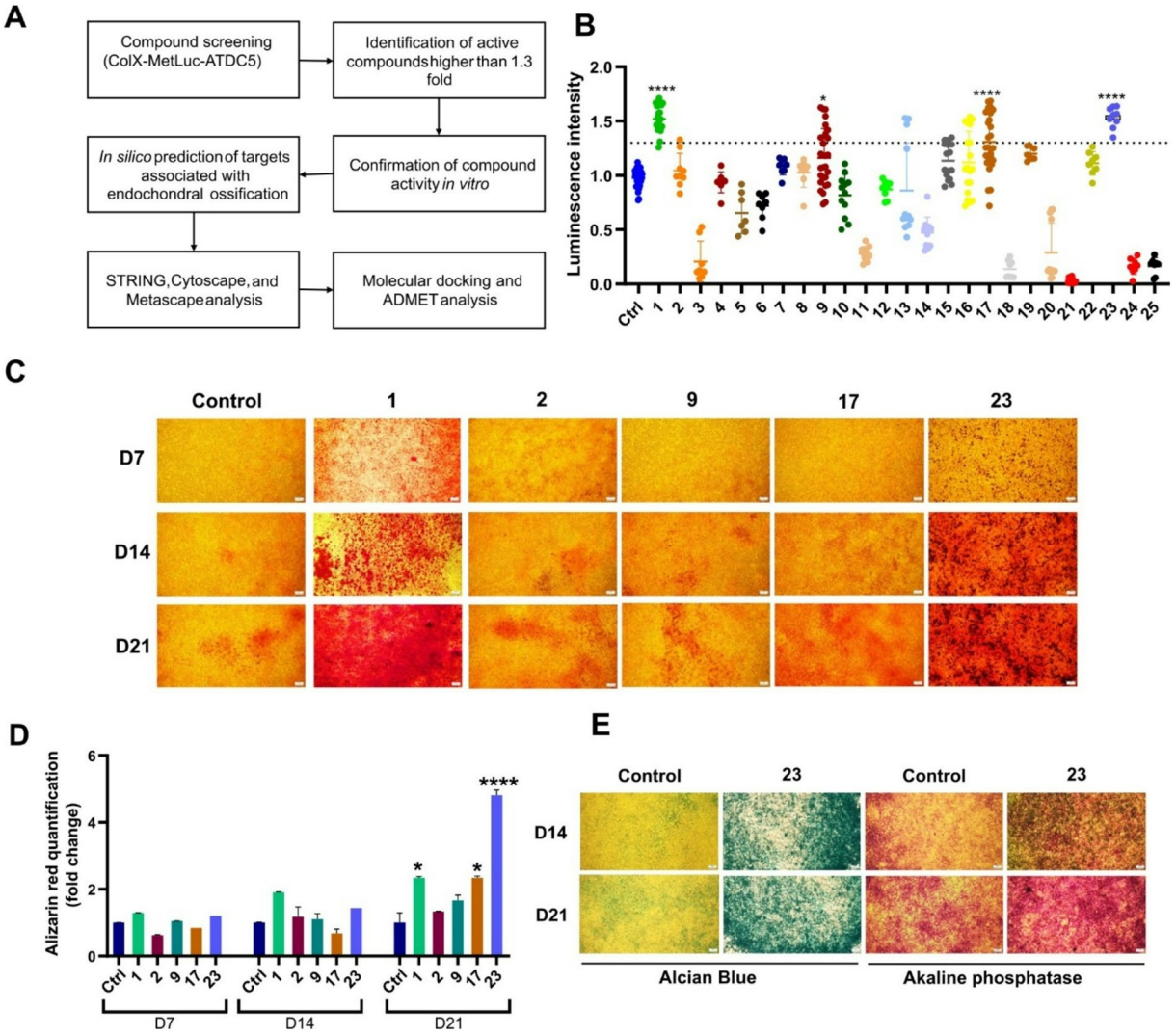

Fig. 4. Identification of active compounds on chondrocyte hypertrophy. **(A)** Flow chart of the procedure. **(B)** Scatter plot of the luciferase-based screening in ATCD5-ColX cells at 24 h (at least eight independent experiments). ATDC5-ColX cells were seeded at a density of 2×10^4 cells in a 96-well plate, cultured in chondrogenic medium, and treated with leucettamine B, nacryline and their derivatives. Luminescence was detected using a microplate luminometer. Data are presented as mean ± SD. Statistical analysis was performed using one-way ANOVA followed by Dunnett's multiple comparisons test versus control. Statistical significance was assessed for all conditions; however, only compounds inducing a significant increase compared to control are indicated. Significance levels are defined as follows: $^*p < 0.05$, and $^{****}p < 0.0001$.**C)** Chondrocytes extracellular matrix mineralization. ATDC5 cells were seeded in micromass 3D model at a density of 10^5 cells in a drop of 10 µL, cultured in chondrogenic medium for 21 days, and treated with leucettamine B (**1**), nacryline (**2**), pinctazole (**23**), and two nacryline analogues (9 and 17) before Alizarin red staining. Mineralization was observed under a light microscope (ZEISS axiovert). Data represent three independent experiments. **(D)** Quantification of calcified red nodules with acetic acid and ammonium hydroxyde. The absorption was measured at 425 nm and results are represented as a fold of control of three independent experiments. Statistical analysis was performed using one-way ANOVA followed by Dunnett's multiple comparisons test versus control. Significance levels are indicated as follows: $^*p < 0.05$, and $^{****}p < 0.0001$.**(E)** Evaluation of matrix production and differentiation following treatment with pinctazole by staining with Alcian blue and alkaline phosphatase on days 14 and 21. Data represent two independent experiments.

of their ability to promote chondrocyte hypertrophic differentiation and mineralization, assessed by Alizarin red staining. Among them, leucettamine B (**1**) and compound **23**, later named pinctazole, significantly increased the extracellular matrix (ECM) mineralization after three weeks of treatment (Fig. 4C), indicating their capacity to stimulate chondrocyte differentiation until the terminal state. Notably, pinctazole (**23**) showed superior activity, resulting in a 5-fold increase in calcium nodules (Fig. 4D), suggesting greater calcium deposition at D21 compared to compound **1**. To further support these results, Alcian blue and alkaline phosphatase (PAL) staining were performed at days 14 and 21. At day 14, treatment with pinctazole (**23**) led to an increase of

the glycosaminoglycan production, while a significant increase of PAL was also observed suggesting enhanced hypertrophic activity (Fig. 4E). These findings suggest that pinctazole (**23**) has the potential to stimulate hypertrophy.

Given that this compound is derived from nacryline (**2**) and shares structural similarities with leucettamine B (**1**), we selected the three compounds for in silico mechanistic studies to predict their differential biological effects.

In silico potential targets identification and PPI analysis

Using Swiss Target Prediction and Super-PRED databases, 428, 440, and 398 targets were predicted for leucettamine B, nacryline and pinctazole, respectively, based on their SMILES codes (Table S1). Targets related to "endochondral ossification (EO)" were then filtered using the CTD (Comparative Toxicogenomics Database) and represented in a Venn diagram. There were 21, 23, and 27 intersecting targets associated with EO for leucettamine B (**1**), nacryline (**2**), and pinctazole (**23**), respectively (Fig. 5A, B and C).

The protein-protein interaction (PPI) network for the intersecting targets of each compound was then built in functional protein association network STRING and exported to Cytoscape_v3.10.3 for visual analysis. Nodes located outside the network were eliminated. Although leucettamine B (**1**) and nacryline (**2**) share structural similarities, the network shows a total of 20 interacting targets for both compounds, among which five were common (CCND1, NFKB1, KLF5, FGFR1 and KDR). The PPI networks constructed from the predicted targets of leucettamine B (1), nacryline (2), and pinctazole (23) contained 99, 24, and 133 edges, respectively(Fig. 5D, E and F). In line with our in vitro results, these data suggest that these compounds have different biological effects.

Interestingly, the network of pinctazole (**23**) has more nodes (25) and edges (133) than that of nacryline (**2**), from which it is derived (Fig. 5F), indicating a more complex network of predicted protein-protein interactions. This may help explain the different biological responses observed in our in vitro assays (Fig. 4B, C and D).

It is well known that proteins with more linkers can play a crucial role in the network and are more implicated in component-disease or component-biological process correlations. In other words, they are more likely to be targeted by pharmacological treatments[17]. In this manner, the topological parameters of each compound-targeted-gene were analyzed using the CytoNCA plug-in, and the medians of their betweenness centrality, closeness centrality, and degree of centrality were calculated (Table S2). The analysis yielded medians, used as cardinal values, and targets that are above these medians were selected for further in silico analysis (Table S3).

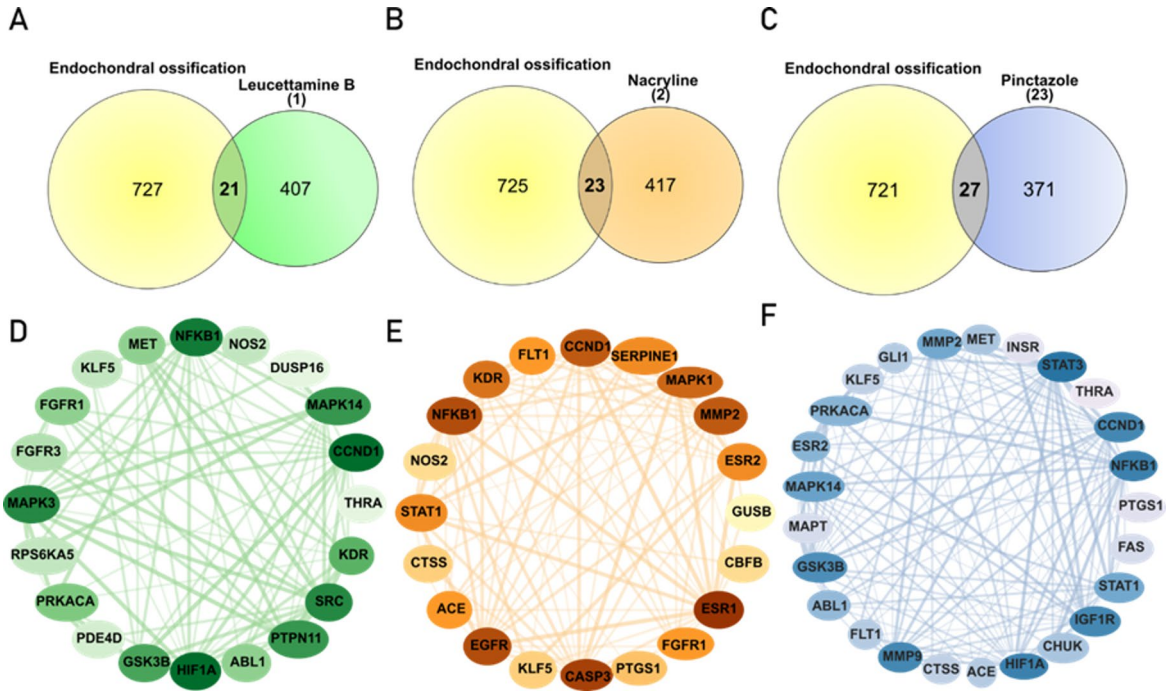

Fig. 5. Network pharmacology analysis. Venn diagram showing the number of overlapping between endochondral ossification proteins and **(A)** targets of leucettamine B (**1**) **(B)** targets of nacryline (**2**) **(C)** targets of pinctazole (**23**). **(D**, **E**,**F)** The pharmacological PPI network of the key targets was represented in green for (**1**), orange for (**2**), and blue for (**23**). Leucettamine B (**1**) showed 20 interracting targets with 84 edges, nacryline showed 20 interracting targets with 99 edges, and pinctazole showed 25 nodes and 133 edges. Nodes were colored based on their topological parameters, with darker shades indicating a higher degree of connectivity for the node.

KEGG and GO enrichment analysis of Pinctazole (23)

In order to understand the mechanisms underlying the effects of the active compound, pinctazole, on the endochondral ossification process, we performed KEGG and GO enrichment. The key targets listed in Table S3 were analyzed in Metascape.

Consistent with the PPI network, this compound has different mechanisms than leucettamine B (**1**) and nacryline (**2**) (Fig. 6; S2; S3). The key targets of pinctazole (**23**) can affect 233 biological pathways that mainly regulate receptor tyrosine kinase signaling pathways (RTK), cell migration and growth, and protein binding (Fig. 6A). Studies showed that migration and condensation of mesenchymal stem cells (MSC) to the bone surface are important for endochondral bone formation and fracture healing[18]. It is well documented that out of 58 RTKs known in the human genome, 10 are associated with chondrocyte hypertrophy, an essential stage of endochondral ossification[19].

In the molecular functions, 23 pertinent entries were enriched, mainly linked to protein kinase binding and activity, phosphotransferase activity, and transcription factor binding (Fig. 6B). Regarding the cellular components, 10 relevant entries were enriched, primarily associated with the transcription regulator complex, protein kinase complex, and glutamatergic synapse (Fig. 6C). KEGG pathway, revealed 88 pathways associated with cancer, prolactin, HIF-1 signaling, FoxO signaling, Ras signaling, MAPK, and PI3K-AKT pathways (Fig. 6D). These pathways affect chondrocyte activity in different ways. For instance, Seriwatanachai et al. showed that prolactin regulates chondrocyte proliferation, differentiation, and apoptosis[20]. It was also demonstrated that prolactin modulates chondrogenic activity and leads to increased endochondral ossification in lactating rats[21]. HIF-1 signaling was demonstrated to be crucial in regulating chondrocyte differentiation during endochondral ossification, and its up-regulation results in significant growth of long bones[22]. Some MAPK members such as c-Raf, MEK1/2, and ERK1/2 are required for the expression of collagen X, a marker for hypertrophic chondrocyte[23]. PI3K/Akt signaling is known as a regulator of the terminal chondrocyte differentiation. Furthermore, inhibition of PI3K/AKT reduced bone growth by decreasing chondrocyte proliferation and hypertrophy[24–26].

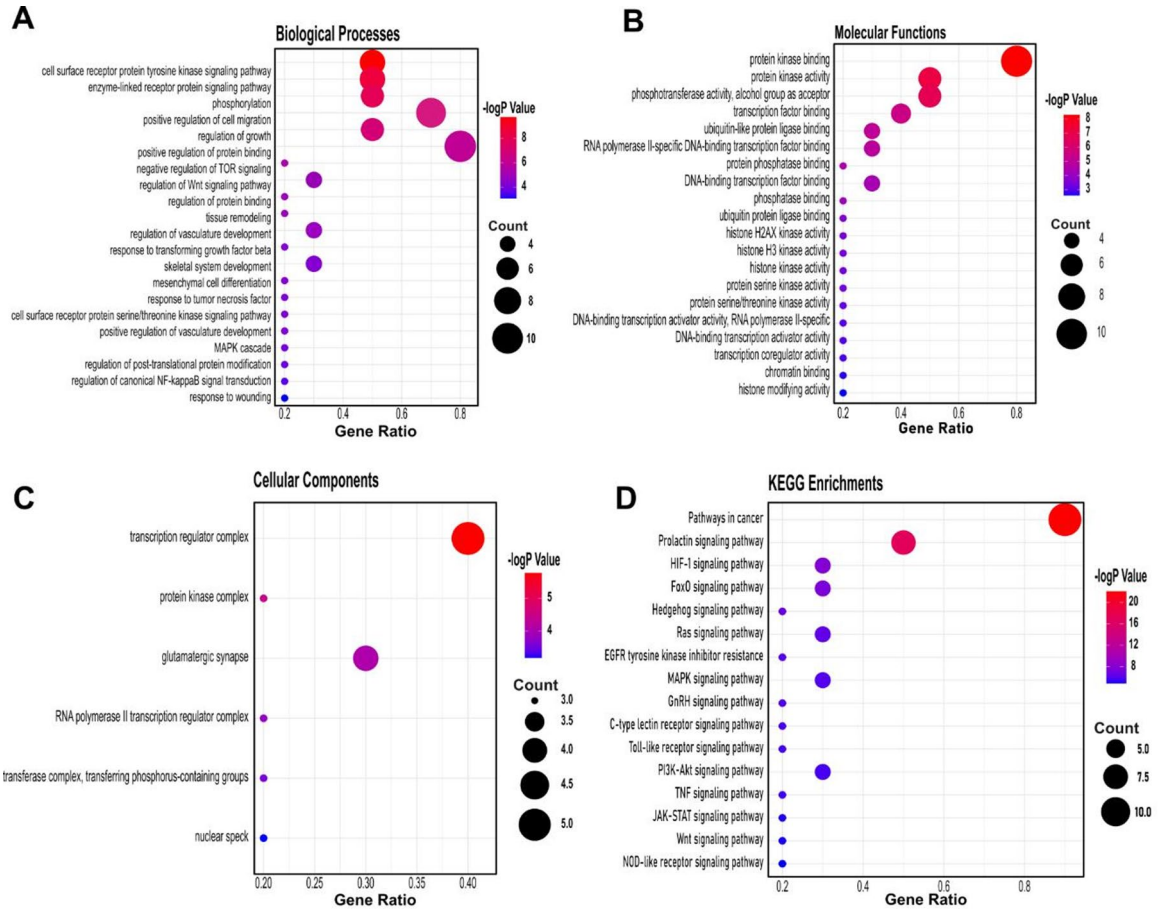

Fig. 6. Gene ontology and Kyoto encyclopedia of genes and genomes enrichment analysis of the top targets of pinctazole (23). **(A)** Biological Processes, (B) Molecular Functions, **(C)** Cellular Components, **(D)** and KEGG enrichment. Data were visualized in R studio. The gene ratio represents the number of genes implicated in a specific pathway or function over the total number of genes. The size of the count dot corresponds to the number of implicated genes. Significance is represented as the -logP value.

KEGG enrichment also predicts an association with pathways in cancer. This was not unexpected given the huge publicly available data on oncology studies. KEGG enrichment and GO were used to predict the mechanism of action of pinctazole (**23**) on endochondral bone formation.

Contrary to the aforementioned results, leucettamine B (**1**) regulates biological pathways involved in regulating cellular responses to cytokines, intracellular transport, mTOR signaling, and cell surface receptor protein tyrosine kinase signaling (Fig. S2). At the molecular function level, it primarily regulates protein kinase activity and binding. In terms of cellular components, it mainly affects the glutamatergic synapse as well as membrane microdomains and rafts. KEGG enrichment analysis reveals that this compound is predominantly associated with pathways linked to endocrine resistance and C-type lectin receptor signalling. Similarly, nacryline (**2**) also exhibits distinct regulatory effects than pinctazole (**23**) (Fig.S3). It modulates biological pathways related to cellular responses to cyclic compounds and lipids, as well as epithelial cell proliferation. At the molecular function level, it primarily regulates protein kinase regulator activity, whereas in cellular components, it is mainly associated with the vesicle lumen. According to KEGG enrichment analysis, nacryline (**2**) is strongly linked to endocrine resistance pathways. These findings highlight the mechanistic variation between these two compounds and pinctazole (**23**), which can support their distinct biological effects.

Molecular docking analysis

The key targets were docked with each compound using Autodock vina 1.1.2. This software uses affinity score to predict the binding capacity. The molecular docking results revealed that pinctazole (**23**) has higher total binding energy – 153.5 kcal/mol than leucettamine B (**1**) (-140.9 kcal/mol) and nacryline (**2**) (-111.6 kcal/mol) (Fig. 7A). It is well known that strong binding activity is indicated by K< -7 kcal/mol[27,28]. Therefore, leucettamine B (**1**) exhibited strong binding affinity to 9 out of 21 targets (MAPK3, Src, MAPK14, KDR, EGFR, ESR1, MAPK1, ESR2, and ABL1) (Fig. 7A, S4). However, nacryline (**2**) revealed weak binding activity to all targets (Fig. 7A, S5). Pinctazole (**23**) showed a robust binding affinity to Src, MAPK14, KDR, and MAPK3.

Among them, Src showed a binding energy of K= -7.3 kcal/mol to leucettamine B (**1**) and K= -8.5 kcal/mol to pinctazole (**23**), suggesting that these composites may stimulate endochondral ossification by regulating Src (Fig. 7A and C). Src is a cytoplasmic non-receptor tyrosine kinase that regulates cell adhesion, survival, proliferation, differentiation, and cytokine receptor activation[29]. From the N-terminus, Src consists of an SH4 unique domain, crucial for membrane attachment, followed by SH3 and SH2 domains, essential for both intramolecular and intermolecular interactions and the regulation of catalytic activity. At the C-terminus, it comprises a protein kinase domain (SH1) (Fig. 7C). Leucettamine B (**1**) forms conventional hydrogen bonds with Src on TYR 93 and ASN 138 residues. These hydrogen interactions stabilize the compound within the binding site by reducing the overall energy of the complex[30]. Additionally, PHE 153 forms a π-π stacking interaction which enhances binding specificity through aromatic interactions. LEU 92 forms a hydrophobic π-alkyl interaction with the ligand. It is well known that hydrophobic interactions play a crucial role in improving ligand-receptor binding[31]. These interactions occur with the SH3 domain of Src. Additionally, leucettamine B (**1**) also interacts strongly with MAKP3, MAPK14, KDR, EGFR, ESR1, MAPK1, ESR2 and ABL2 (Fig. 7A and B).

The molecular docking results showed that pinctazole (**23**), the most active one, could bind to ABL1 which is also a non-receptor tyrosine kinase like Src. Given the structural similarity between this compound and leucettamine B, we hypothesized that pinctazole might also bind to Src. Our results indicates that it could interact with ASP 407 of Src by conventional hydrogen bounds. ASP 407 also makes a π-anion interaction with an aromatic ring of this compound. However, an unfavorable donor-donor interaction between LYS 298 and pinctazole (**23**) suggests a possible electrostatic repulsion. Interestingly, hydrophobic interactions, such as π-σ and π-alkyl interactions, are observed with LEU 396, VAL 284, LEU 276, THR 341, ALA 296, ILE 339, VAL 326, and ALA 406 of Src and pinctazole (**23**), contributing to the stabilization of the complex and strengthening van der Waals forces with LEU 410, MET 317, LEU 328, MET 344, TYR 343 and GLY 347 (Fig. 7C). Interestingly, these interactions are established with the SH1 protein kinase domain. It is worth noting that pinctazole (**23**) interacts strongly with NFKB1, MAPK3, PTPN11, MAPK14, GSK3B, KDR, PRKACA, EGFR, ESR1, MAPK1, MMP2, ESR2, IGF1R, STAT3, MMP9, and ABL1 (Fig. 7A and B). It is also important to highlight that biological activity was assessed on mouse pre-chondrogenic ATCD5 cells, whereas molecular docking was done on human Src. To address possible species-specific variations, human Src and mice Src sequences were aligned to examine the domain conservation, and we found that the binding site of pinctazole (**23**) was conserved across both species (Fig. S6). Since Src showed the strongest interactions with this compound, it can be considered its most representative target for regulating the endochondral ossification process. Previous studies have reported that a decrease in FAK/Src signaling is a crtitical step permitting chondrogenic differentiation[32]. Also, Src activity can suppress osteoblast maturation through inhibition of Runx2[33]. Therefore, if pinctazole would be able to inhibit Src activity, this interaction could potentially contribute to the promotion of chondrogenesis and bone formation. However, further experimental studies are needed to confirm the Pinctazole-Src interaction and to determine whether this compound indeed modulates Src activity.

Evaluation of drug-likeness and ADME-related properties of pinctazole (23)

Drug-likeness describes the degree to which a compound displays molecular and structural properties consistent with known pharmaceutical agents. Assessment of drug-likeness involves evaluating parameters such as hydrophobicity, electronic distribution, hydrogen bonding capacity, and molecular weight[34]. Lipinski's Rule of Five (RO5), and Veber rules, are both of the widely used guidelines for predicting solubility and permeability that are crucial for an effective absorption and penetration of the compound. Compounds that violate these rules are more expected to have poor absorption and permeability, which can reduce their potential as orally bioavailable candidate drugs[35,36]. To assess these properties, pinctazole (**23**) was analyzed using SwissADME. As shown in Table 1, this compound obeys with both Lipinski and Veber rules criteria. It presents a lipophilicity

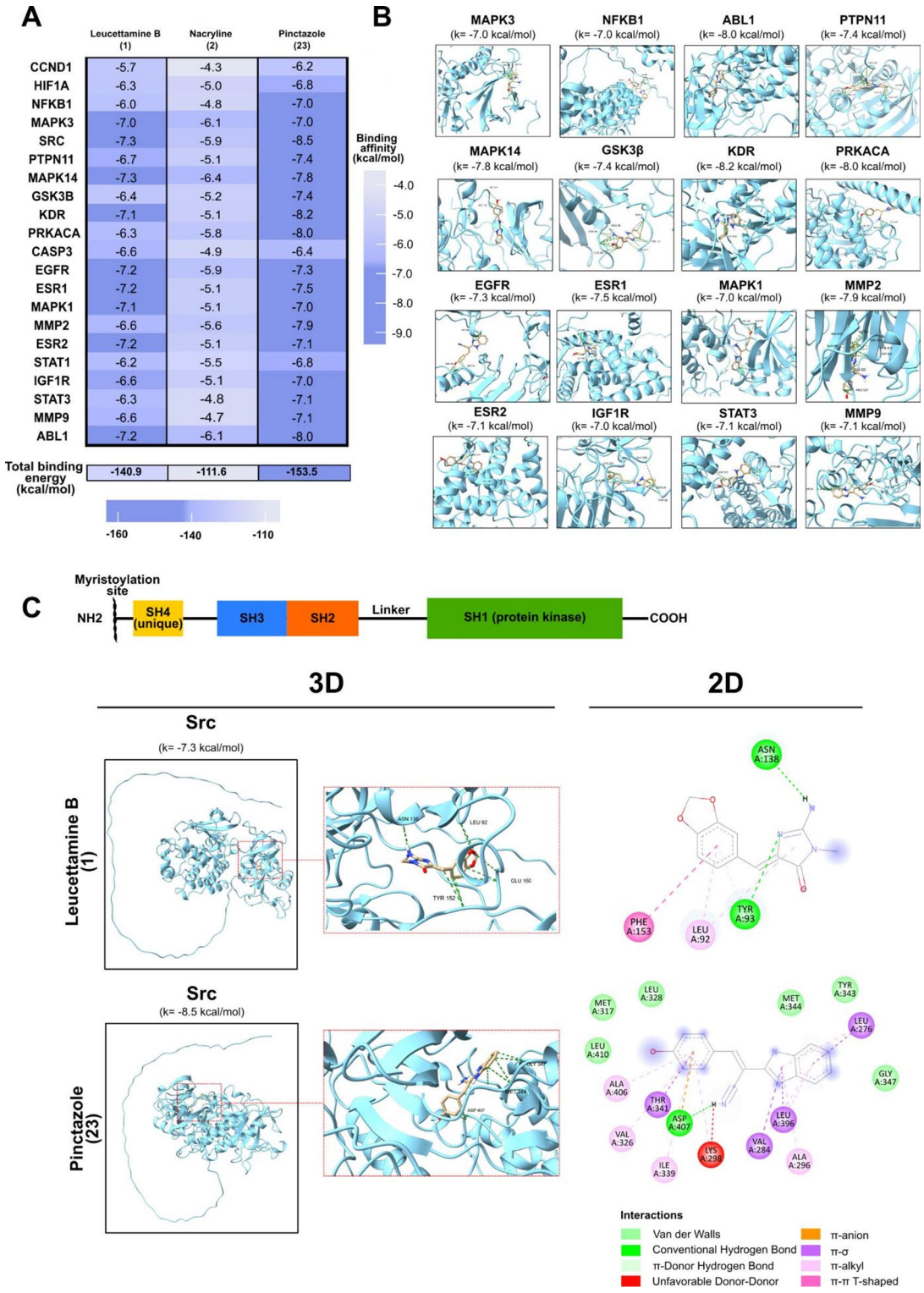

Fig. 7. Molecular docking and coupling visualization. **(A)** Graphic representation of the binding affinity (K) of each compound to the key targets and their total binding affinity in kcal/mol. K<-7 kcal/mol indicates higher binding affinity. **(B)** Coupling of pinctazole (**23**) to its high-affinity targets. (**C**) 2D and 3D visualization of pinctazole (**23**) coupling to Src. Leucettamine B (**1**) establishes hydrogen bounds with ASN198, TYR93 and hydrophobic bounds with LEU92 and PHE153, while pinctazole (**23**) establishes hydrogen bound with ASP407, hydrophobic interactions with LEU276, LEU396, ALA296, VAL284, THR341, VAL326, ILE339, ALA406 and Van der Walls interactions with LEU410, MET317, LEU328, MET344, and TY343.

Compound	Molecular weight (g/mol)	Lipholicity (logP)	Hydrogen bond donors	Hydrogen bond acceptors	Topological Polar Area Surface (TPAS) Å²	Number of rotable bonds
Pinctazole	261.28	2.59	2	3	72.7	2
	≤ 500	≤ 5	≤ 5	≤ 10	≤ 140	≤ 10
	Lipinski (RO5)				Veber rule	

Table 1. Drug-likeness properties of pinctazole (23). RO5 indicates lipinski's rule of five and states that an orally active drug should have a molecular weight below 500 Da, a logP of less than five, no more than five hydrogen bounds donors and acceptors. Veber's rule states that, for better oral bioavailability, the topological polar area surface of the compound should be 140 Å² or less with ten of fewer rotable bonds.

Property	Model Name	Predicted Value	Unit
Absorption	Water solubility	-2.988	Numeric (log mol/L)
	Caco2 permeability	0.847	Numeric (log Papp in 10^{-6} cm/s)
	Intestinal absorption (human)	83.21	Numeric (% Absorbed)
	Skin Permeability	-2.735	Numeric (log Kp)
	P-glycoprotein substrate	Yes	Categorical (Yes/No)
	P-glycoprotein I inhibitor	No	Categorical (Yes/No)
	P-glycoprotein II inhibitor	Yes	Categorical (Yes/No)
Distribution	VDss (human)	1.157	Numeric (log L/kg)
	Fraction unbound (human)	0	Numeric (Fu)
	BBB permeability	-0.588	Numeric (log BB)
	CNS permeability	-1.958	Numeric (log PS)
Metabolism	CYP2D6 substrate	Yes	Categorical (Yes/No)
	CYP3A4 substrate	No	Categorical (Yes/No)
	CYP1A2 inhibitior	Yes	Categorical (Yes/No)
	CYP2C19 inhibitior	Yes	Categorical (Yes/No)
	CYP2C9 inhibitior	Yes	Categorical (Yes/No)
	CYP2D6 inhibitior	Yes	Categorical (Yes/No)
	CYP3A4 inhibitior	Yes	Categorical (Yes/No)
Excretion	Total Clearance	0.874	Numeric (log ml/min/kg)
	Renal OCT2 substrate	Yes	Categorical (Yes/No)

Table 2. ADME properties of pinctazole (23). Data were generated using pkCSM pharmacokinetics software.

(log P) of 2.59 and an Abbott score greater than zero indicating its capacity to cross the cell membrane, to bind to Src intracellularly and being bioavailable (Tables 1 and 2). Thus, pinctazole (**23**) proved adequate drug-likeness characteristics in silico.

Determining pharmacological properties is crucial to reduce the time required for drug development and improving its success. The ADMET characteristics of pinctazole (**23**) were evaluated using pkCSM-

pharmacokinetics tool (Table 2). This compound shows acceptable gastrointestinal absorption and crosses the blood-brain barrier permeability. However, it presents a low skin permeability (log kp -2.735). P-glycoprotein is a drug-transporter. It acts by favoring drug metabolism and limiting its cellular uptake. Our results suggest that pinctazole (**23**) may be a substrate of P-glycoprotein.

The steady-state volume of distribution (VDss) is a theoretical volume at which a drug has completed the distribution between central and peripheral compartments[37]. The optimal VDss values are between 0.71 L/kg and 2.81 L/kg. Herein, pinctazole (**23**) showed a VDss of 1.157 L/kg, indicating its appropriate distribution.

Cytochrome P450 (CYP450) is a group of enzymes that are crucial for the detoxification of xenobiotics. Drugs can either stimulate or inhibit CYP450 or do not affect it. When prescribing a drug known to be a CYP450 inhibitor or inducer, we must be careful and vigilant to avoid drug-drug interactions. The pharmacokinetics prediction analysis suggests that pinctazole (**23**) may act as an inhibitor of CYP1A2, CYP2C19, CYP2C9, CYP2D6, and CYP3A4. However, further experimental verification is needed to assess its effects at different concentrations.

Regarding its excretion, this compound seems to be an organic cation transporter 2 (OCT2) substrate. OCT2 is involved in the uptake of xenobiotics from the bloodstream into the kidney. Additionally, pinctazole (**23**) showed an acceptable clearance of 0.874 ml/min/kg. Overall, such results suggest that this compound may have efficient pharmacological properties. However, these data remain predictive and require validation through in vitro and in vivo experiments to confirm the pharmacokinetics of pinctazole (**23**), particularly by assessing its efficacy at various concentrations and determining the threshold at which it could present adverse effects to avoid potential side effects.

Conclusion

This study focuses on targeting and stimulating the early first steps of endochondral ossification. Through cell-based screening of natural products and their synthetic analogs, three compounds were identified. Among them, pinctazole (**23**), derived from nacryline (**2**), showed a high capacity to stimulate hypertrophy of ADTC5 cells and matrix mineralization. Consistent with these findings, the network pharmacology showed that the three compounds may act differently and among them pinctazole (**23**) has multiple targets and can regulate several pathways. The molecular docking results revealed that this compound may have a high binding affinity to several receptors, especially to the non-receptor tyrosine kinase protein Src with a binding affinity of k= -8.5 kcal/mol. This kinase is predicted to be the optimal target of pinctazole (**23**) for stimulating the EO process. Furthermore, the ADME analysis showed that this compound may hold favorable pharmacological properties and compliance with Lipinski's and Veber's rules. The physiological properties indicate that pinctazole (**23**) may exhibit high absorption through the gastrointestinal tract, and showed an efficient cell membrane permeability, distribution, and excretion. However, although the ATDC5 micromass model allowed the investigation of early events of EO associated with chondrocyte hypertrophy and matrix mineralization, it does not fully recapitulate the complex processes occurring during fracture healing[38,39]. Therefore, further in vivo studies, particularly in fracture healing models, will be required to confirm the role of pinctazole (23) in endochondral bone repair and to evaluate its safety and therapeutic potential.

Materials and methods

General material and methods

All reagents were of commercial grade and were used without further purification, unless otherwise stated. Commercially available anhydrous solvents were used for reactions conducted under inert atmosphere. Reagent grade solvents were used in all other cases. Organic solvents were purchased from Thermo Fisher Scientific. All other chemicals were purchased from Aldrich or Fluorochem. Reported yields are unoptimized.

Medium-Pressure Liquid Chromatography (MPLC) was performed on a Puriflash apparatus using Silica gel Interchim cartridge PF-50SIHP (Interchim, Montluçon, France). The synthesis reactions were monitored by thin-layer chromatography (TLC). The TLC was performed on aluminum pre-coated silica gel 60 F254 plates, visualized by UV light (254 nm) and revealed with a solution of sulfuric vanillin. Preparative HPLC purifications were performed on an autoprep system: Waters 600 controller and Waters 600 pump with a Waters 996 photodiode array detector (Waters Corporation, Milford, USA), equipped with a Waters Sunfire C18 (19 × 150 mm, 5 µm) column.

Nuclear magnetic resonance (^{1}H and^{13} C NMR) spectra were recorded with a Bruker AVANCE 300 or a Bruker AVANCE 500 spectrometer. Proton NMR spectra are referenced from the residual proton in the NMR solvent ($CDCl_3$: δ_H 7.26, MeOD: δ_H 3.31). Data are reported as follows: chemical shift [multiplicity (s = singlet, d = doublet, t = triplet, q = quartet, m = multiplet), coupling constant(s) in Hertz, integration]. Carbon-13 NMR spectra are referenced from the carbon resonances of the solvent ($CDCl_3$: δ_C 77.16, MeOD δ_C 49.00). High resolution mass spectra (HRMS) were recorded on a Waters LCT Micromass spectrometer in positive electrospray ionization - time of flight (ESI-TOF) mode.

Optical rotations were measured using an Anton Paar MCP-300 polarimeter (Anton Paar France, Les Ulis, France) and are reported as follows: $[\alpha]_D^{T\,°C}$ (c = g/100 mL, solvent). Infrared data were obtained with a PerkinElmer Spectrum 65 spectrophotometer using an attenuated total reflectance (ATR) device (n in cm^{-1}).

When crystals were obtained, RX diffraction pattern were recorded. For each of them, a suitable crystal was selected, mounted on a nylon loop and fixed with oil. Then, X-ray diffraction and crystallographic data were collected at room temperature or at 150 K, using redundant w scans on an Rigaku XtaLabPro single-crystal diffractometer using microfocus Mo Kα radiation and a HPAD PILATUS3 R 200 K detector.

Using Olex2[40], the structures were readily solved by intrinsic phasing methods (SHELXT[41], and by full-matrix least-squares methods on F2 using SHELXL[42]. The non-hydrogen atoms were refined anisotropically, and hydrogen atoms, most of them were identified in different maps and were treated as riding on their parent atoms.

Animal material

Sponge *Pericharax orientalis*.

The sponge was collected by hand using SCUBA in Wallis & Futuna, during the sampling cruise Wallis 2018 aboard the R/V Alis[14], in the Wallis Island lagoon (13°16.177'S, 176°08.120'W) at a depth of 15 m on July 2018. The collected sponges were immediately frozen after collection. A voucher sample has been deposited at the Queensland Museum (Brisbane, Australia) under the access number G339027 and was identified by Dr. Merrick Ekins as *Pericharax orientalis*[43] The sponge was deep frozen on board until work up. It was then ground, freeze-dried, and extracted.

Nacre of the pearl oyster *Pinctada margaritifera*.

Nacre powder (particle size 50–100 mm) was prepared from the pearl oyster shell *Pinctada margaritifera* from French Polynesia. Nacre part was isolated from shells of pearl oysters as a by-product of the pearl culture industry. The nacre was grinded by StanSea.

Extraction and isolation

The freeze-dried sponge sample of *Pericharax orientalis* (93 g) was extracted three times by ASE at 40 °C under pressure (100 bar) with a mixture of CH_2Cl_2/MeOH 1:1. The extracts were combined and dried under reduced pressure to afford a brown residue (6 g) and 5.5 g of this residue was partitioned between n-BuOH and H_2O. The butanolic extract (1.4 g) was fractionated by reversed-phase C18 flash chromatography, eluting successively with solvents (H_2O; H_2O/CH_3CN gradient; CH_3CN; CH_2Cl_2; THF) to afford fractions F1 to F3.

Fraction F2 (H_2O/CH_3CN gradient) was purified by preparative reversed-phase HPLC (column: Waters Sunfire C_{18}, 19 mm × 150 mm, 5 mm, H_2O + 0.1% formic acid/CH_3CN + 0.1% formic acid) to obtain 1.2 mg of leucettamine B (**1**).

Analytical and spectroscopic data are in agreement with the literature data[8,44].

Nacre powder (1.5 kg) was stirred with 2.2 L of dichloromethane for 1 h at room temperature and filtered on celite and glass fiber filters. The residue was reextracted 3 times, in 2.2 L of dichloromethane for 2 × 2 h and then overnight. The combined extracts were concentrated under vacuum. The operation on 1.5 kg was repeated 6 times to extract 9 kg of nacre powder and afford a yellow oil (480 mg).

The crude extract was fractionated by flash chromatography on silica gel (column 25 g, gradient from 100% heptane to 100% dichloromethane to DCM/MeOH 85:15 followed by a washing with a mixture EtOAc/acetone/water/formic acid 5:3:0.5:0.5) to afford fractions F1 to F7.

Fraction F5 was purified by preparative reversed-phase HPLC (column: Waters Sunfire C_{18}, 19 mm × 150 mm, 5 mm, H_2O + 0.1% formic acid/CH_3CN + 0.1% formic acid) to obtain 1.2 mg of nacryline (**2**).

Analytical and spectroscopic data are in agreement with the literature data[45].

Synthetic chemistry

The synthetic chemistry is described in the supplementary informations. Using HPLC, all the tested compounds were confirmed to be at 95% pure. HPLC traces are reported in the supplementary informations.

Cell culture

Pre-chondrogenic ATDC5 cells derived from mouse differentiating culture of AT805 tetracarcinoma were cultured in a growth medium consisting of (1:1 Dulbecco's modified Eagle's medium (DMEM): Ham's F-12 (Sigma Aldrich, D6421) mix containing 1% (vol/vol) antibiotic-antimycotic (Gibco, 15240062), 5% foetal bovine serum (Gibco, A5256701), 10 μg/mL human transferrin (Sigma Aldrich, T8158) and 30 nM sodium selenite (Sigma Aldrich, S5261). Cells were maintained in a humidified atmosphere of 5% CO_2 at 37 °C.

Extracts/compounds solubilization

Each compound was dissolved in growth culture medium to prepare a 10 mg/mL stock solution, which was subsequently diluted to the desired working concentrations. Compounds were tested at a final concentration of 0.2 mM, as this concentration was previously used in our earlier studies with nacre and sponge-derived extracts, where it was shown to produce significant biological effects without affecting cell viability[6,7,46].

Biological screening

Since collagen X is a marker of hypertrophic chondrocytes, the human Col X promoter-luciferase reporter plasmid was constructed to study the endochondral bone formation as described previously[7]. The human ColX promoter–luciferase reporter plasmid (ColX-pMetLuc) was constructed by subcloning the upstream promoter region of the human ColXa1 gene (-2979/+21) into pMetLuc2-Reporter plasmid (CLONTECH®, TaKaRa). A stably transfected monoclonal cell line resistant to neomycin (G418, 200 µg/ml, Sigma G418) was created by transfecting Col X-Luc into ATDC5 cell line. One clone was selected between 9 clones obtained after checking the ability to secrete luciferase after stimulation and to differentiate. ColX-pMetLuc-ATDC5 cells were seeded at a density of 2×10^4 cells in 96-well plates, cultured in induction medium consisting of growth medium supplemented with 10 µg/mL insulin (Sigma Aldrich, I0516), and treated with the compounds at the final concentration of 0.2 mM. Control wells received the same induction medium but without the tested compounds. After 24 h, the supernatant was recovered and the luciferase activity was measured using the Ready-To-Glow™ Secreted Luciferase Reporter Assay-Takara according to the manufacturer's instructions.

ATDC5 micromass model

Micromass cultures of ATDC5 cells were grown to study chondrocyte hypertrophic differentiation as described previously[7]. Three droplets of 10^6 cells concentrated in 10 μL were placed in the center of each well and allowed to adhere for 4 h at 37 °C. Then, chondrogenic medium consisting of induction medium supplemented with 50 μg/mL ascorbic acid-2-phosphate and 10 mM β-glycerophosphate was added. Micromasses were cultured for 7, 14, and 21 days, in the presence or not of different compounds. Control wells received the same chondrogenic medium but without the tested compounds. The medium was changed every two days and the corresponding treatments were freshly added at each medium change.

Extracellular matrix characterization

Alcian blue (Sigma Aldrich, TMS-010) was used to assess glycosaminoglycan formation within the extracellular matrix, Alizarin red (Sigma Aldrich, A5533) and phosphatase alkaline (Sigma Aldrich, SCR004) staining were used to assess its mineralization. After 7, 14 and 21 days, micromasses fixed with 4% paraformaldehyde for 30 min at 4 °C and incubated with 1% (w/v) Alizarin red solution or Alcian blue or PAL for 5 min. After staining, the cells were washed with demineralized water to remove excess staining solution. Stained micromasses were observed under a light microscope (ZEISS Axiovert).

For mineralization quantification after alizarin red staining, 10% of acetic acid (Sigma Aldrich 695092) was added to the cells and incubated at room temperature for 30 min. Cells were gently scraped and lysates were heated at 85 °C for 10 min and then centrifuged for 15 min at 4 °C. The supernatant was recovered and treated with 10% ammonium hydroxide (Sigma Aldrich 221228), and the absorbance was measured at 425 nm using a microplate reader TECAN Infinite M-PLEX.

Targets predictions

The sequences of the leucettamine B (**1**), nacryline (**2**) and pinctazole (**23**) were converted to SMILES structures using OpenBabel tool. Target predictions were made by Swiss Target Prediction, Super-PRED and pharmmapper databases, and duplicates were removed. Relevant targets associated with endochondral ossification were obtained from CTD database, and protein IDs were converted to gene IDs using UniProt ID mapping. The intersection between compound targets and EO targets was obtained through Venny online.

Network analysis

The protein-protein interaction network was constructed using STRING database and exported to Cytoscape 3.10.3 software for analysis. The species selected was Homo Sapiens and nodes with no interactions were removed from the network. Topological parameters including degree, betweenness centrality, and closeness centrality of the leucettamine B (**1**), nacryline (**2**) and pinctazole (**23**) were determined using CytoNCA plug-in. Values above the medians were selected for further investigation.

Gene Ontology (GO) and Kyoto Encyclopedia of Genes and Genomes (KEGG) enrichment analysis

Key targets selected from Cytoscape were imported into Metascape online database for analysis. The components of GO biological process (BP), GO cellular components (CC), GO molecular functions (MF) and KEGG pathway enrichment analysis were performed, and data were exported to RStudio for visualization and DotPlot generation.

Molecular docking

The PDB structures of the key targets were downloaded from AlphaFold database. The chemical structures of the compounds were converted to PDB structures using OpenBabel online tool. Proteins and ligands were prepared and converted to PDBQT using Autodock tools 1.57. Molecular docking was then performed using AutoDock Vina as described by Zhu et al.[47]. Docking results were visualized using ChimeraX and Discovery Studio.

Prediction of drug-likeness and pharmacological properties (ADME)

Drug-likeness properties of pinctazole including hydrophobicity, molecular weight, hydrogen bond, and electronic distribution, were predicted using SwissADME tool. Pharmacological properties were determined using pkCSM pharmacokinetics software (https://biosig.lab.uq.edu.au/pkcsm/) which gives information about the pharmacokinetics (Absorption, Distribution, Metabolism, and Excretion (ADME)) of this compound.

Statistical analysis

Statistical analyses were performed using GraphPad Prism 9 (GraphPad Software, USA). Comparisons between multiple groups were conducted using one-way analysis of variance (ANOVA) followed by Dunnett's multiple comparisons test versus control. Statistical significance was defined as $p < 0.05$. Data are presented as mean ± SD from the independent experiments, as indicated in the corresponding figures.

Data availability

The datasets generated and/or analysed during the current study are available in the ZENODO repository, permanent access link is following: https://doi.org/10.5281/zenodo.18265617.

Received: 15 December 2025; Accepted: 1 April 2026
Published online: 21 April 2026

References

1. Rivera, K. O. et al. Local injections of β-NGF accelerates endochondral fracture repair by promoting cartilage to bone conversion. *Sci. Rep.* **10**, 1–15 (2020).
2. Wozney, J. M. The bone morphogenetic protein family and osteogenesis. *Mol. Reprod. Dev.* **32**, 160–167 (1992).
3. Carroll, A. R., Copp, B. R., Grkovic, T., Keyzers, R. A. & Prinsep, M. R. Marine natural products. *Nat. Prod. Rep.* **41**, 162–207 (2024).
4. Zhang, G. et al. Nacre, a natural, multi-use, and timely biomaterial for bone graft substitution. *J. Biomed. Mater. Res. A.* **105**, 662–671 (2017).
5. Iandolo, D. et al. Preclinical safety study of nacre powder in an intraosseous sheep model. *BMJ Open. Sci.* **6**, 100231 (2022).
6. de Muizon, C. J., Iandolo, D., Nguyen, D. K., Al-Mourabit, A. & Rousseau, M. Organic Matrix and Secondary Metabolites in Nacre. *Mar. Biotechnol.* **24**, 831–842 (2022).
7. de Jourdain, C. et al. Chemical Investigation of the Calcareous Marine Sponge Pericharax heteroraphis, Clathridine-A Related Derivatives Isolation, Synthesis and Osteogenic Activity. *Mar. Drugs*. **22**, 196 (2024).
8. Chan, G. W. et al. New Leukotriene B_4 Receptor Antagonist: Leucettamine A and Related Imidazole Alkaloids from the Marine Sponge Leucetta microraph is. *J. Nat. Prod.* **56**, 116–121 (1993).
9. Carreaux, F. et al. An Efficient Method for the Preparation of New Analogs of Leucettamine B under Solvent-Free Microwave Irradiation. *Heterocycles* **78**, 1191 (2009).
10. Molina, P., Almendros, P. & Fresneda, P. M. An iminophosphorane-mediated efficient synthesis of the alkaloid leuce ttamine B of marine origin. *Tetrahedron Lett.* **35**, 2235–2236 (1994).
11. Roué, N. & Bergman, J. Synthesis of the marine alkaloid leucettamine B. *Tetrahedron* **55**, 14729–14738 (1999).
12. Loaëc, N. et al. Marine-Derived 2-Aminoimidazolone Alkaloids. Leucettamine B-Related Po lyandrocarpamines Inhibit Mammalian and Protozoan DYRK & CLK Kinases. *Mar. Drugs*. **15**, 316 (2017).
13. Hsu, M. H. et al. Leucettamine B analogs and their carborane derivative as potential anti-cancer agents: Design, synthesis, and biological evaluation. *Bioorg. Chem.* **98**, 103729 (2020).
14. Petek, S. WALLIS 2018 cruise. *Alis R/V*. https://doi.org/10.17600/18000524 (2018). doi:10.17600/18000524.
15. Tian, H. et al. Pyrrole-Assisted and Easy Oxidation of Cyclic α-Amino Acid- Derived Di ketopiperazines under Mild Conditions. *Adv. Synth. Catal.* **353**, 1525–1533 (2011).
16. Wells, G., Seaton, A. & Stevens, M. F. G. Structural Studies on Bioactive Compounds. 32. Oxidation of Tyrphostin Protein Tyrosine Kinase Inhibitors with Hypervalent Iodine Reagents. *J. Med. Chem.* **43**, 1550–1562 (2000).
17. Janani, B. et al. A network-based pharmacological investigation to identify the mechanistic regulatory pathway of andrographolide against colorectal cancer. *Front. Pharmacol.* **13**, 967262 (2022).
18. Su, P. et al. Mesenchymal Stem Cell Migration during Bone Formation and Bone Diseases Therapy. *Int. J. Mol. Sci.* **19**, 2343 (2018).
19. Ferrao Blanco, M. N., Garcia, D., Legeai-Mallet, H. & Van Osch, G. J. L. V. M. Tyrosine kinases regulate chondrocyte hypertrophy: promising drug targets for Osteoarthritis. (2021). https://doi.org/10.1016/j.joca.2021.07.003 doi:10.1016/j.joca.2021.07.003.
20. Seriwatanachai, D., Krishnamra, N. & Charoenphandhu, N. Chondroregulatory action of prolactin on proliferation and differentiation of mouse chondrogenic ATDC5 cells in 3-dimensional micromass cultures. *Biochem. Biophys. Res. Commun.* **420**, 108–113 (2012).
21. Suntornsaratoon, P., Wongdee, K., Krishnamra, N. & Charoenphandhu, N. Possible chondroregulatory role of prolactin on the tibial growth plate of lactating rats. *Histochem. Cell. Biol.* **134**, 483–491 (2010).
22. Qin, Q. et al. Hypoxia-Inducible Factors Signaling in Osteogenesis and Skeletal Repair. *Int. J. Mol. Sci.* **23**, 11201 (2022).
23. Papaioannou, G. et al. Raf Kinases Are Essential for Phosphate Induction of ERK1/2 Phosphorylation in Hypertrophic Chondrocytes and Normal Endochondral Bone Development. *J. Biol. Chem.* **292**, 3164–3171 (2017).
24. Ulici, V., Hoenselaar, K. D., Gillespie, J. R. & Beier, F. The PI3K pathway regulates endochondral bone growth through control of hypertrophic chondrocyte differentiation. *BMC Dev. Biol.* **8**, 1–15 (2008).
25. Wolfgart, J. M. et al. Biomarkers for hypertrophic chondrocyte differentiation are associated with spatial cellular organisation and suggest endochondral ossification-like processes in osteoarthritic cartilage: An exploratory study. *J. Orthop. Translat.* **48**, 232–243 (2024).
26. Kita, K., Kimura, T., Nakamura, N., Yoshikawa, H. & Nakano, T. PI3K/Akt signaling as a key regulatory pathway for chondrocyte terminal differentiation. *Genes Cells*. **13**, 839–850 (2008).
27. Ferreira, L. G., Santos, D., Oliva, R. N., Andricopulo, A. D. & G. & Molecular docking and structure-based drug design strategies. *Molecules* **20**, 13384–13421 (2015).
28. Hu, H. Y. et al. Hesperidin anti-osteoporosis by regulating estrogen signaling pathways. *Molecules* **28**, 6987 (2023).
29. Hall, A. P., Westwood, F. R. & Wadsworth, P. F. Review of the Effects of Anti-Angiogenic Compounds on the Epiphyseal Growth Plate. *Toxicol. Pathol.* **34**, 131–147 (2006).
30. Chen, X., Li, X. & Li, Y. Toxicity inhibition strategy of microplastics to aquatic organisms through molecular docking, molecular dynamics simulation and molecular modification. *Ecotoxicol. Environ. Saf.* **226**, 112870 (2021).
31. Lai, H. et al. Interformer: an interaction-aware model for protein-ligand docking and affinity prediction. *Nat. Commun.* **15**, 1–12 (2024).
32. Matsubara, T., Yasuda, K., Mizuta, K., Kawaue, H. & Kokabu, S. Tyrosine Kinase Src Is a Regulatory Factor of Bone Homeostasis. *Int. J. Mol. Sci. 2022.* **23**, 5508 (2022).
33. Pala, D. et al. Focal Adhesion Kinase/Src Suppresses Early Chondrogenesis CENTRAL ROLE OF CCN2 *. *J. Biol. Chem.* **283**, 9239–9247 (2008).
34. Gheidari, D., Mehrdad, M. & Karimelahi, Z. Virtual screening, ADMET prediction, molecular docking, and dynamic simulation studies of natural products as BACE1 inhibitors for the management of Alzheimer's disease. *Sci. Rep.* **14**, 1–11 (2024).
35. Lipinski, C. A., Lombardo, F., Dominy, B. W. & Feeney, P. J. Experimental and computational approaches to estimate solubility and permeability in drug discovery and development settings. *Adv. Drug Deliv Rev.* **64**, 4–17 (2012).
36. Veber, D. F. et al. Molecular properties that influence the oral bioavailability of drug candidates. *J. Med. Chem.* **45**, 2615–2623 (2002).
37. Jantarawong, S., Wathanaphanit, P., Panichayupakaranant, P. & Pengjam, Y. Prediction of ADMET profile and anti-inflammatory potential of chamuangone. *Sci. Rep.* **15**, 1–15 (2025).
38. Wilhelm, D., Kempf, H., Bianchi, A. & Vincourt, J. B. ATDC5 cells as a model of cartilage extracellular matrix neosynthesis, maturation and assembly. *J. Proteom.* **219**, 103718 (2020).
39. Bragdon, B., Lybrand, K. & Gerstenfeld, L. Overview of Biological Mechanisms and Applications of Three Murine Models of Bone Repair: Closed Fracture with Intramedullary Fixation, Distraction Osteogenesis, and Marrow Ablation by Reaming. *Curr. Protoc. Mouse Biol.* **5**, 21 (2015).
40. Dolomanov, O. V., Bourhis, L. J., Gildea, R. J., Howard, J. A. K. & Puschmann, H. OLEX2: a complete structure solution, refinement and analysis program. *urn:issn:0021-8898* **42**, 339–341 (2009).
41. Sheldrick, G. M. SHELXT – Integrated Space-Group and Crystal-Structure Determination. *Acta Crystallogr. Found. Adv.* **71**, 3–8 (2015).
42. Sheldrick, G. M. Crystal Structure Refinement with SHELXL. *Acta Crystallogr. C Struct. Chem.* **71**, 3–8 (2015).
43. Galitz, A. et al. Molecular genetic biodiversity assessment of the Wallis Island sponge fauna in the Tropical Pacific. *J. Mar. Biol. Association United Kingd.* **104**, e56 (2024).

44. Dražić, T., Molčanov, K., Jurin, M. & Roje, M. Synthesis of marine alkaloids leucettamines B and C by β-lactam ring r earrangement. *Synth. Commun.* **47**, 764–770 (2017).
45. Erdman, P. J., Gosse, J. L., Jacobson, J. A. & Lewis, D. E. The Reaction of Hydrazine with α-Cyanocinnamate Esters: A Caveat. *Synth. Commun.* **34**, 1163–1171 (2004).
46. Brion, A. et al. Nacre extract restores the mineralization capacity of subchondral osteoarthritis osteoblasts. *J. Struct. Biol.* **192**, 500–509 (2015).
47. Zhu, H., Zhou, R., Cao, D., Tang, J. & Li, M. A pharmacophore-guided deep learning approach for bioactive molecular generation. *Nat. Commun.* **14**, 1–11 (2023).

Acknowledgements

We thank his majesty Lavelua Takumasiva Aisake, King of Wallis, and the territorial authorities for allowing us to collect in their country, Atoloto Malau and Florian Le Bail from the Wallis and Futuna Environment service, for their help and assistance. We acknowledge the crew of the R/V ALIS and IRD's diving team (SEOH IRD Noumea, New Caledonia) for their essential contribution to the Wallis 2018 oceanographic cruise. We thank Merrick Ekins as well as Dirk Erpenbeck for the identification of the sponges. We also would like to thank all the laboratories, SAINBIOSE, ICSN, LEMAR and MATEIS for their help and all the technical facilities that enabled us to carry out this work.

Author contributions

CJM and CM: synthesis and chemical characterization; SN and CE: activity assays, and statistical analyses, SN: *in silico* analyses ; SP: Collection of the sponges materials, CJM, SN, AAM and MR: Write and review the manuscript. All authors have read and agreed to the published version of the manuscript.

Funding

This work is part of CJM's PhD thesis. We acknowledge the financial support of the doctoral school ED 488 SIS as well as the NADO project funded by the ANR JCJC program (ANR18-CE18-0003-01). The Wallis 2018 oceanographic cruise was funded by the French Oceanographic Fleet, IRD, MNHN, Labex Mer and the Wallis and Futuna Environment Service. We acknowledge INSERM, CNRS, IRD, and Jean Monnet University for their financial support.

Declarations

Competing interests

MR is one of the co-founders of the Stansea company and provides scientific consultation for Megabiopharma.

Additional information

Supplementary Information The online version contains supplementary material available at https://doi.org/10.1038/s41598-026-47546-y.

Correspondence and requests for materials should be addressed to M.R.

Reprints and permissions information is available at www.nature.com/reprints.

Publisher's note Springer Nature remains neutral with regard to jurisdictional claims in published maps and institutional affiliations.